Editors' Suggestion

Inertial forces for particle manipulation near oscillating interfaces

Siddhansh Agarwal,[1] Bhargav Rallabandi,[2,*] and Sascha Hilgenfeldt[1,†]
[1]*Department of Mechanical Science and Engineering, University of Illinois at Urbana-Champaign, Urbana, Illinois 61801, USA*
[2]*Department of Mechanical and Aerospace Engineering, Princeton University, Princeton, New Jersey 08544, USA*

(Received 28 April 2018; published 4 October 2018)

Due to the inherent nonlinearity of fluid dynamics, a large class of oscillating flows gives rise to rectified effects of steady motion. It has recently been shown that particle transport in such flows leads to differential displacement and efficient sorting of microparticles. Here we present a model that generalizes a Maxey-Riley-like equation for particle motion, incorporating important viscous and inviscid effects near oscillating interfaces and efficiently bridging the acoustofluidic and microfluidic approaches. Resulting in direct predictions for particle motion on slower timescales, the model predicts a richer and qualitatively different behavior from that expected from simplified radiation-force formalisms: depending on experimental control parameters, the net effect of interfacial oscillation can be either an attraction to or a repulsion from the interface, and particles can be captured at a fixed distance or released. These results are verified in comparison with experiments.

DOI: 10.1103/PhysRevFluids.3.104201

I. INTRODUCTION

Despite the prevalence of small Reynolds numbers, inertia has recently been acknowledged as an important player in microfluidics applications. Inertia has been discussed extensively in two main contexts: the inertial migration of particles due to steady shear flow gradients [1,2], and acoustofluidics, where the particle is exposed to the oscillatory flow in acoustofluidic waves; see, e.g., Ref. [3]. While acoustofluidic forces are used in applications and are well understood in the inviscid limit for particles in isolation [4], different theories with contradictory predictions about the magnitude and direction of forces have been proposed when viscous effects become important [5,6].

More recently, a third complex of microfluidics applications has been discussed that is concerned with particles in incompressible flows near oscillating interfaces. Perhaps the simplest class of these flows is set up by cylindrical or spherical bubbles of radius a_b that oscillate with a small amplitude $\epsilon a_b, \epsilon \ll 1$. Particles near such bubbles often get attracted towards the interface [7–9], while in other situations differential repulsion has been noted [10–13]. Related work concerns acoustic interactions between bubble-driven microswimmers [14]. In many of these cases, attractive forces have been attributed semiquantitatively to the "secondary radiation force" (SRF) on a spherical particle in the far field of a radial standing acoustic wave [15–17]. This effect has been discussed in a variety of scenarios (see Refs. [18,19]), but there has been no attempt, to the authors' knowledge, to systematically include force contributions beyond SRF or unify this concept with that of repulsive

*Current affiliation: Department of Mechanical Engineering, University of California Riverside, Riverside, California 92521, USA.
†sascha@illinois.edu

forces. In the context of particles near oscillating interfaces, the unmodified use of SRF may not be appropriate, as the particle is not in a standing acoustic far field but is exposed to an incompressible oscillatory flow that is strongly influenced by the nearby interfacial geometry as well as by viscous effects.

Numerous publications [5,6,20,21] have described the force on a particle in an acoustic setting, but they do not capture the effect of a nearby interface and/or assume a very specific form of the background flow field. In the spirit of previous work [22], the present work incorporates the aforementioned effects in the context of a Maxey-Riley-like formalism [23], aiming for a flexible tool to efficiently predict particle motion in a variety of oscillating flows. Section II generalizes a previous approach of timescale separation to incorporate important density-dependent and inertial effects. In Sec. III we discuss the predicted impact of the effects on particle manipulation (attraction or repulsion). Section IV compares the results with a specific set of experimental data and elucidates previously unexplained phenomena for particles near interfaces. In Sec. V it is pointed out that, even far from interfaces, the present formalism agrees with, and sheds light on, inviscid and viscous versions of acoustofluidic forces. Conclusions are presented in Sec. VI.

II. PARTICLE EQUATION OF MOTION NEAR AN INTERFACE

In order to address the issues alluded to above we have proposed an approach [22] where the motion of a particle near an oscillating interface is modeled by a modified version of the Maxey-Riley equation [23], which is an ordinary differential equation (ODE) for motion of a rigid sphere (radius a_p, density ρ_p) of mass $m_p = (4/3)\pi\rho_p a_p^3$ placed in a general incompressible, known background flow field $\mathbf{u}(\mathbf{r}, t)$ (present without the particle). The current work aims at incorporating additional effects into this Maxey-Riley approach and derive the rectified particle motion on timescales longer than the oscillation period for a wide variety of scenarios, in order to assess the qualitative and quantitative impact on the particle position dependent on parameters like density contrast, particle size, or driving frequency. Despite the wider scope, we aim to maintain the character of an explicit equation of motion for the position of the particle center $\mathbf{r}_p(t)$, in which the known flow field $\mathbf{u}$, together with its derivatives, is instantaneously evaluated at $\mathbf{r}_p(t)$. In particular, this excludes nonlocal or history effects. This approach necessitates additional approximations but yields a versatile equation that can be readily applied to a multitude of situations and yields straightforward ODE solutions for particle trajectories.

Following Ref. [24], we will decompose the hydrodynamic force into inviscid and viscous contributions $\mathbf{F}^H = \mathbf{F}_i^H + \mathbf{F}_v^H$ and discuss additional effects that modify these terms in the case of our interest.

A. Correction terms and approximations

The original derivation of Maxey and Riley [23] is valid for a spherical particle of radius a_p with small inertia; specifically, (1) the particle Reynolds number based on a typical *difference* velocity between particle speed and background flow must be small, and (2) the background flow must satisfy the small Stokes number condition $a_p^2 U_0/(\nu L_0) \ll 1$, where U_0 and L_0 are the velocity and gradient scales of $\mathbf{u}$, respectively, and ν the kinematic viscosity. In specializing the problem to periodic flows induced by the oscillation with angular frequency ω of an interfaces with finite curvature scale (e.g., a bubble of radius a_b), we identify $L_0 = a_b$ and $U_0 = \epsilon a_b \omega$, so that the latter condition can be written as $\epsilon\lambda \ll 1$, where we define the inertial parameter $\lambda = \frac{1}{3}\frac{a_p^2\omega}{\nu}$ [22]. A third, natural condition is (3) assuming the particle to be small compared to the scale of the interface, i.e., $a_p/a_b \ll 1$.

A consequence of the oscillatory nature of the flows is that time averages of first-order forces in ϵ will vanish, while second-order rectified terms will persist as steady effects. In particular, $O(\epsilon^2)$ inertial effects are not necessarily negligible (for appreciable Reynolds number of the primary oscillating flow), so that an original approximation from Ref. [23] neglecting second-order terms in $\mathbf{F}_i^H$ involving the perturbation flow induced by the presence of the particle is not generally valid.

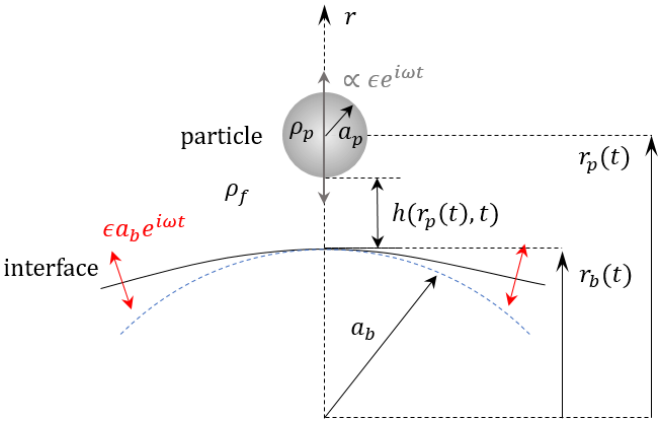

FIG. 1. Problem setup and nomenclature for a spherical particle of radius a_p near an oscillating interface (curvature length scale a_b).

In Ref. [24] the effect of such terms was worked out; in addition to the terms of advective inertia already present in the Maxey-Riley equation, and using $m_f = m_p\rho_f/\rho_p$, this yields

$$\mathbf{F}_i^H \approx -\frac{1}{2}m_f\left(\frac{d\mathbf{v}_p}{dt} - \frac{D\mathbf{u}}{Dt}\right) + m_f\frac{D\mathbf{u}}{Dt} + \frac{1}{3}m_f a_p^2\nabla\mathbf{u} : \nabla(\nabla\mathbf{u}), \tag{1}$$

where the last term on the right-hand side represents the second-order effect of the perturbation flow. This term will turn out to be of considerable, and sometimes dominant, size for small distances between the particle and the oscillating interface, which is the main interest of this study. A term proportional to $\nabla^2\mathbf{u}$ has been neglected, as the primary oscillatory flow (of appreciable Reynolds number) is nearly irrotational, so that $\nabla^2\mathbf{u}$ is negligible.

The proximity of the interface also introduces important modifications in the viscous part of the force, as was previously shown in Ref. [22]. It is well known that the viscous hydrodynamic force on a sphere depends on the distance to the interface, interpolating between the usual Stokes drag far away and a lubrication expression nearby [25]. In Ref. [22] the forces were appreciable only at a very small separation distance, so that the expression was always dominated by lubrication drag. However, here we will be concerned with both small and large separation distances; therefore, we acknowledge in the model that the action of the viscous lubrication term in the oscillatory flow is confined to separation distances less than the Stokes boundary layer thickness $\delta_S = \sqrt{2\nu/\omega}$. This confinement has been described in various oscillating-flow lubrication problems with both no-slip and stress-free interfaces [26–28]. For an interface of characteristic radius of curvature a_b, we identify the center of curvature with the origin (see Fig. 1) and combine the Stokes and lubrication expressions [22], so that

$$\mathbf{F}_v^H \approx -6\pi\nu\rho_f a_p\left\{\frac{d\mathbf{r}_p}{dt} - \mathbf{u} + H\left[\frac{h(\mathbf{r}_p,t)}{\delta_S}\right]\frac{a_p\left(\frac{d\mathbf{r}_p}{dt}\cdot\mathbf{e}_r - \frac{\partial r_b}{\partial t}\right)}{n_B h(\mathbf{r}_p,t)}\mathbf{e}_r\right\}, \tag{2}$$

where $r_b(\theta,t)$ is the radial position of the point on the oscillating interface nearest the particle and $h(\mathbf{r}_p,t) = \mathbf{r}_p\cdot\mathbf{e}_r - r_b - a_p$ used in the lubrication term is the separation distance between the surfaces of particle and interface (see Fig. 1). The integer n_B depends on the boundary condition at the interface: $n_B = 1$ for no-slip, and $n_B = 4$ for no-stress (the case pursued for oscillating bubbles in this work). The decay of the lubrication force outside the boundary layer is modeled by the exponential $H(z) = \exp(-z)$, consistent with the literature [27–29]. Expression (2) neglects Faxén-term contributions proportional to $\nabla^2\mathbf{u}$, consistent with the above approximations. We also assume

that there is negligible feedback on $r_b(\theta, t)$ from the particle's presence (small capillary numbers due to particle motion; see Ref. [30])

Both (1) and (2) also omit contributions from the Basset-Boussinesq history force. These are known to be negligible in a number of relevant situations [31–33]. For the current case of harmonic oscillatory flows, the history integral becomes an explicit expression if (a) transients have died out and (b) the leading-order oscillatory motion of the particle is harmonic translation in bulk. For this particular case, the history term reduces to well-established correction terms in (1) and (2) [34,35] of order $\lambda^{-1/2}$, which are negligible in the limits of both large and small viscous effects. While assumption (a) is sustainable, we focus here on forces on particles not in bulk, but near an interface, so that we omit these terms altogether and defer a discussion to Sec. V, where we evaluate forces at a large distance from the interface.

Another effect of order $\lambda^{-1/2}$ is the Saffman lift for particles traversing shear gradients, considered, e.g., in Chong *et al.* [31]; in the present work, we will exclusively deal with particles moving parallel to the flow field and thus omit this term. In summary, we shall use

$$\mathbf{F}^H \approx -6\pi\nu\rho_f a_p \left[\left(\frac{d\mathbf{r}_p}{dt} - \mathbf{u} \right) + H\!\left(\frac{h}{\delta_S} \right) \frac{a_p \left(\frac{d\mathbf{r}_p}{dt} \cdot \mathbf{e}_r - \frac{\partial r_b}{\partial t} \right)}{n_B h(\mathbf{r}_p, t)} \mathbf{e}_r \right] - \frac{1}{2} m_f \left(\frac{d^2\mathbf{r}_p}{dt^2} - \frac{D\mathbf{u}}{Dt} \right) + m_f \frac{D\mathbf{u}}{Dt} + \frac{1}{3} m_f a_p^2 \nabla\mathbf{u} : \nabla(\nabla\mathbf{u}) \tag{3}$$

as our approximation for the force governing particle motion near an interface. Defining dimensionless variables $\tilde{\mathbf{r}}_p = \mathbf{r}_p/a_b$, $\tilde{t} = \omega t$, and $\tilde{\mathbf{u}} = \mathbf{u}/U_0$, we use (3) to obtain an ordinary differential equation that describes a wide variety of oscillatory particle dynamics,

$$\lambda(\hat{\kappa} + 1) \frac{d^2\tilde{\mathbf{r}}_p}{d\tilde{t}^2} + \left[\mathbf{I} + H\!\left(\frac{\tilde{h}}{\tilde{\delta}} \right) \frac{\gamma \mathbf{e}_r \mathbf{e}_r}{\tilde{h}(\tilde{\mathbf{r}}_p, t)} \right] \cdot \frac{d\tilde{\mathbf{r}}_p}{d\tilde{t}} = \epsilon \left[\lambda \left(\frac{\partial \tilde{\mathbf{u}}}{\partial \tilde{t}} + \epsilon \tilde{\mathbf{u}} \cdot \tilde{\nabla} \tilde{\mathbf{u}} \right) + \frac{2}{9} \epsilon \lambda n_B^2 \gamma^2 \tilde{\nabla} \tilde{\mathbf{u}} : \tilde{\nabla}\left(\tilde{\nabla} \tilde{\mathbf{u}} \right) + \tilde{\mathbf{u}} + H\!\left(\frac{\tilde{h}}{\tilde{\delta}} \right) \frac{\gamma}{\tilde{h}(\tilde{\mathbf{r}}_p, \tilde{t})} \frac{\partial \tilde{r}_b}{\partial \tilde{t}} \mathbf{e}_r \right]_{\tilde{\mathbf{r}}_p}, \tag{4}$$

where we have introduced $\gamma \equiv a_p/(n_B a_b) \ll 1$ and $\tilde{\delta} = \delta_S/a_b$, and the density contrast $\hat{\kappa} = \frac{2}{3}(\frac{\rho_p}{\rho_f} - 1)$, while $\tilde{h}(\tilde{\mathbf{r}}_p, t) = \tilde{r}_p - \tilde{r}_b - n_B\gamma$ is the dimensionless particle-interface separation distance. Our discussion goes beyond Ref. [22] because (4) contains additional correction terms and because we will not restrict ourselves to $\hat{\kappa} = 0$. Thus, the dynamics of the particle $\tilde{\mathbf{r}}_p(\tilde{t})$ depend on moments of the undisturbed background fluid velocity at the particle center, the motion of the bubble interface, and the independent dimensionless parameters ϵ, γ, $\hat{\kappa}$, $\tilde{\delta}$, and n_B; we note that λ is related to these by $\lambda = 2/(3n_B^2\gamma^2\tilde{\delta}^2)$.

B. Timescale separation and the radial problem

The most extensive set of quantitative experimental data available for comparison (see Sec. IV) concerns an interface with almost purely radial oscillations. Thus, we project (4) onto the radial direction and obtain a simpler equation using the radial velocity $\tilde{u}$. Such a purely radial oscillation does not give rise to any steady streaming flow [36], so that the nontrivial rectification effects of particle motion studied here can be studied in isolation from streaming transport, which in more general flows would be a further consequence of the oscillations. We do allow for an externally imposed steady Lagrangian component of flow $\epsilon\tilde{u}_L$ in addition to the oscillatory $\tilde{u}_{\rm osc}$, so that $\tilde{u} = \tilde{u}_{\rm osc}(r, \tau) + \epsilon\tilde{u}_L(r) = \tilde{u}_0(r)e^{i\tilde{t}} + \epsilon\tilde{u}_L(r)$, where $\tilde{u}_0(r)$ is the spatial dependence of the oscillatory part. The factor ϵ anticipates the relative scaling of these flows. We make analytical progress using timescale separation, introducing the slow timescale $\tilde{T} = \epsilon^2\tilde{t}$ and expanding (4) to second order in

ϵ, seeking a solution as

$$\tilde{r}_p(\tilde{t},\tilde{T}) = \tilde{r}_{p_0}(\tilde{t},\tilde{T}) + \epsilon\tilde{r}_{p_1}(\tilde{t},\tilde{T}) + \epsilon^2\tilde{r}_{p_2}(\tilde{t},\tilde{T}) + \cdots . \tag{5}$$

The procedure follows Ref. [22] closely, taking into account the additional terms, extracting a leading-order equation for $\tilde{r}_{p_0}$ dependent on the slow scale $\tilde{T}$ only (the scale $\tilde{t}$ is averaged out). Details of the derivation are found in Appendix.

In the following, we will drop all tildes for clarity. The resulting equation is an overdamped (first order in time) ODE for the particle position representing a quasisteady force balance involving only the instantaneous undisturbed flow field:

$$-F_D = F_R + F_\rho + F_{i,2} \equiv F_\lambda, \tag{6}$$

where

$$F_D = u_L - \frac{h_0 + H_0\gamma}{h_0}\frac{dr_{p_0}}{dT},$$

$$F_R = H_0\gamma\lambda\frac{[-1+u_0(r_{p_0})]u_0'(r_{p_0})}{2}\frac{h_0(\hat{\kappa}+2)+H_0\gamma}{(h_0+H_0\gamma)^2+h_0^2\lambda^2(\hat{\kappa}+1)^2},$$

$$F_\rho = \hat{\kappa}\lambda\frac{u_0(r_{p_0})u_0'(r_{p_0})}{2}h_0\frac{h_0[\lambda^2(\hat{\kappa}+1)-1]-H_0\gamma}{(h_0+H_0\gamma)^2+h_0^2\lambda^2(\hat{\kappa}+1)^2},$$

$$F_{i,2} = \frac{1}{9}\lambda n_B^2\gamma^2\left\{\frac{2u_0(r_{p_0})}{r_{p_0}^2}\left[u_0'(r_{p_0}) - \frac{u_0(r_{p_0})}{r_{p_0}}\right] + u_0'(r_{p_0})u_0''(r_{p_0})\right\}.$$

Every nondimensional force term can be made dimensional by multiplying with the Stokes drag scale $\mathcal{F}_S \equiv 6\pi\nu\rho_f a_p\epsilon^2 a_b\omega$.

In (6), $h_0 = r_{p0} - 1 - n_B\gamma$ is the average of the separation distance h over an oscillation cycle, $H_0 = H(h_0/\delta)$, and all the flow quantities are evaluated at the particle position. F_D is the drag force acting on the particle, whereas F_R results from inertial rectification terms independent of $\hat{\kappa}$ and repels the particle from the interface if u_0 decays with r (as is physically reasonable for most flow fields). While these two contributions have been explained in a previous publication [22], the last two terms are distinctive to the present work and add attractive forces to the scenario. The force F_ρ is proportional to the density contrast ($\hat{\kappa}$) and particle inertia (λ) parameters; it is attractive for $\hat{\kappa} > 0$ and $\lambda \gtrsim 1$. This term decays more slowly with r near the interface compared to the inertial rectification term and typically overwhelms it at distances $h_0 \geqslant \gamma$. The last term, $F_{i,2}$, represents the inviscid correction of Ref. [24] [the last term in (1)], which always attracts the particle towards the interface regardless of $\hat{\kappa}$ but decays more strongly with r since it depends on higher-order derivatives of the flow field.

Having completed the timescale separation, we verify that the $r_{p_0}(T)$ dynamics resulting from (6) agrees with the full unsteady numerical solution of (4) for a range of parameter combinations (λ, $\hat{\kappa}$, and γ). Anticipating comparison to an experimental situation where a bubble oscillates in a spherical breathing mode, we set $u_0(r) = 1/r^2$, $n_B = 4$ and solve both equations, first assuming $u_L = 0$. Figure 2 illustrates this agreement for two representative cases, showing repulsion for light particles in Fig. 2(a) and attraction towards a fixed-point distance for density-matched particles in Fig. 2(b). The existence of fixed points for r_{p_0} can be assessed by evaluating the net inertial force F_λ. Figure 2(c) graphs F_λ for the two representative cases, showing that the first is unconditionally repulsive ($F_\lambda > 0$ for all r), while the second has a stable fixed point at some surface-to-surface distance h_s, where $dr_{p_0}/dT = 0$.

We can estimate the magnitude of h_s by expanding F_λ for $\lambda \gg 1$, $\gamma \ll 1$, and $|\hat{\kappa}| \ll 1$ (the situation reflecting the most common range of experimental parameters modeled here) and obtain

$$h_s \approx \frac{(2\gamma)^{3/2}}{(32\gamma^2+\hat{\kappa})^{1/2}\lambda}. \tag{7}$$

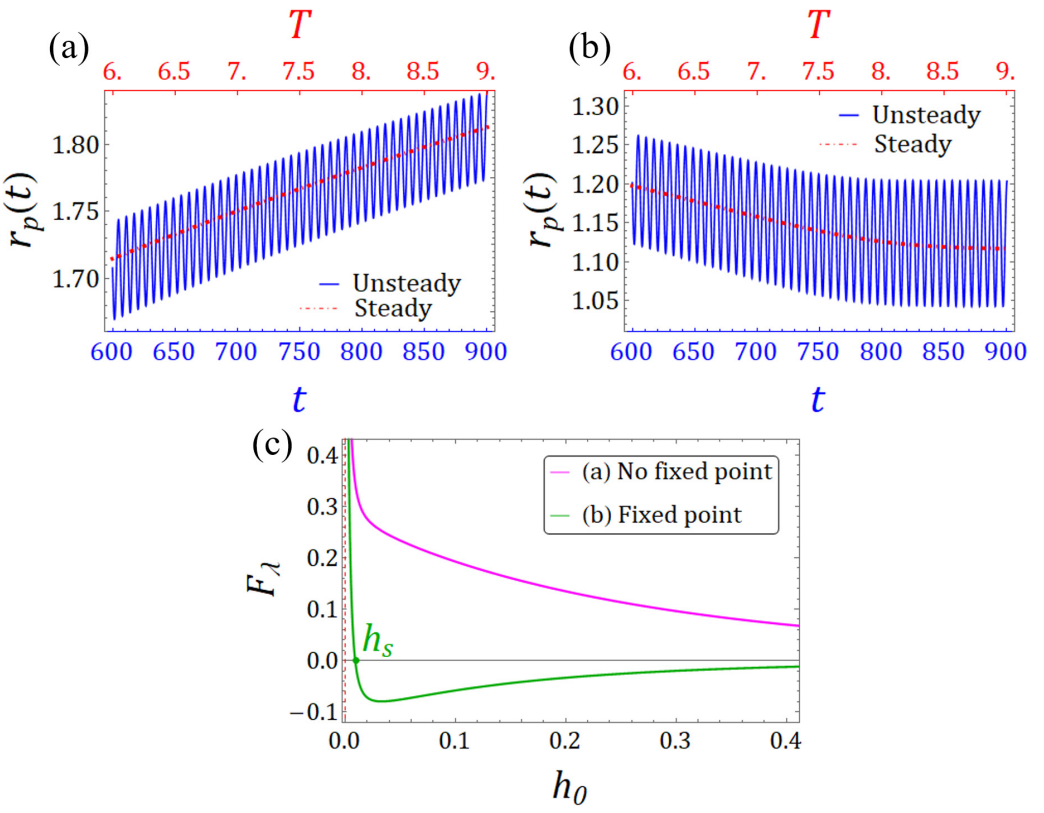

FIG. 2. Comparison of slow-time [steady, Eq. (6)] and oscillatory [unsteady, Eq. (4)] numerical solution for $\epsilon = 0.1$, $\gamma = 0.026$, $r_p(0) = 1.36$, and $r_p'(0) = \epsilon u_0(r_p(0), 0) = 0.054$ (with $u_L = 0$, $n_B = 4$): (a) $\hat{\kappa} = -0.06$ (particle lighter than fluid), $\lambda = 10$; (b) $\hat{\kappa} = 0$ (density matched), $\lambda = 10$; (c) total steady force on the particle as a function of interface separation, showing no fixed points for the repulsive case (a) and a stable fixed point for the attractive case (b).

For approximately density-matched particles this further simplifies to the estimate $h_s \sim \gamma^{1/2}/(4\sqrt{2}\lambda)$. Thus, for typical parameters in oscillator experiments (where often $\lambda \gg 1$) the equilibrium distance is expected to be extremely small compared with the interface scale, and typically even compared with the particle scale. This shows (1) that the inclusion of a lubrication force term is important to explain particle behavior near an equilibrium point and (2) that it should be experimentally feasible to stably position particles at extraordinarily close distances to the interface.

III. PARAMETER DEPENDENCE OF THE FORCES

Since (6) is a first-order ODE, it is easily integrated numerically for many parameter combinations to construct a phase diagram in order to predict the behavior of a particle executing oscillatory motion in a radial flow field (with $u_L = 0$). One expects any such flow field to be dominated by the lowest-order oscillation mode; therefore, as in the above example, we will fix the flow to the monopolar field $u_0 = 1/r^2$ (induced by a spherical bubble in breathing mode, so that $n_B = 4$). The practically relevant question is then whether there is attraction to or repulsion away from the interface depending on parameters. As explained above, the physical distinction is between cases where there are no fixed points (F_λ is always positive and thus repulsive) and cases where a stable fixed point exists [see Fig. 2(c)], with the force being attractive for $h > h_s$. By continuity, there will be a range of parameters in between these cases where two fixed points (one stable, one unstable)

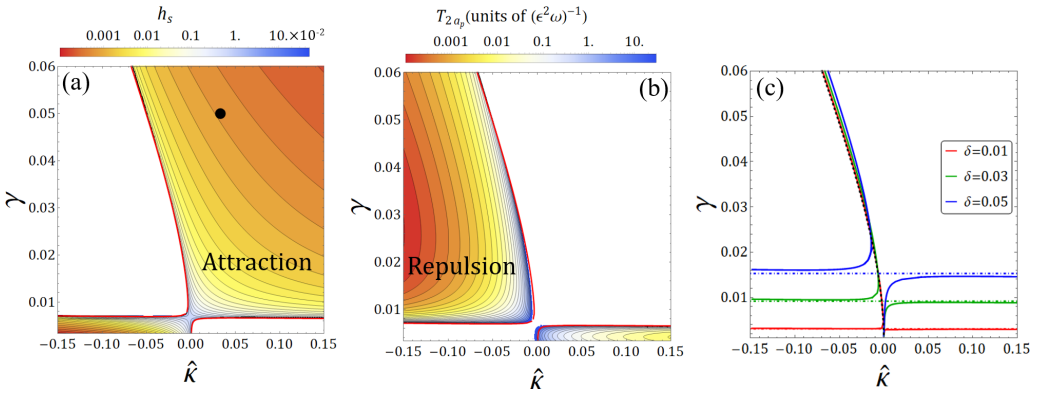

FIG. 3. Phase diagrams of particle behavior as a function of γ and $\hat{\kappa}$; panels (a) and (b) have fixed $\delta = 0.022$. (a) Attractive case: contours indicate the fixed-point equilibrium distance h_s between particle and interface; the red line is the boundary for existence of fixed points from (8). The black dot identifies the experimental parameters of Sec. IV. (b) Repulsive case: contours indicate the time T_{2a_p} for a particle near touching the interface to traverse a distance $2a_p$. (c) Boundary between the attractive and repulsive cases for different δ. The dot-dashed and dashed lines give the analytical predictions based on the sign change of F_ρ and the balancing of the terms F_ρ and $F_{i,2}$, respectively (see the text for more details).

exist so that $F_\lambda < 0$ for a finite range $h_s < h < h_u$ while still $F_\lambda(r \to \infty) > 0$. It can be shown, however, that this regime of a finite range of attraction is small and always closely adjacent to the critical points where $h_s = h_u = h_c$. The latter condition of the double fixed point requires the simultaneous fulfillment of

$$F_\lambda(h_c) = 0, \qquad F'_\lambda(h_c) = 0. \tag{8}$$

In the following phase diagrams, we choose our axes as the easiest parameters to change independently in experiment: particle size (i.e., γ) and density contrast (i.e., $\hat{\kappa}$). The relative importance of viscosity on the particle is quantified by the dimensionless boundary layer thickness $\delta = \sqrt{\frac{2\nu}{a_b^2\omega}}$. We first determine a phase diagram for fixed δ: Finding pairs of $(\gamma, \hat{\kappa})$ values that solve (8) yields the red curves in Figs. 3(a) and 3(b), which show that two separate regions of net repulsion exist (for $\hat{\kappa}$ and γ both small or both large), separated by a contiguous region of attraction. We quantify the behavior in the attractive and repulsive regions differently: In Fig. 3(a) we show the separation distance h_s at the stable fixed point position. Note that these values tend to be very small (small fractions of the oscillator radius a_b and for realistic parameters often in the submicron range). By contrast, for the repulsive region, Fig. 3(b) shows the time [in slow-time units $1/(\epsilon^2\omega)$] required for a particle initially touching the interface to traverse its own diameter $2a_p$. This is a time that may be relevant in experiments in which particles are supposed to be separated by size. As the phase plot shows, these times quickly become very small even a short distance away from the phase boundary between attraction and repulsion. In summary, the forces exerted on the particles effect their displacement quickly and efficiently.

Figure 3(c) demonstrates that this scenario does not qualitatively depend on the exact magnitude of viscous effects (changing δ). Even for much larger $\delta \gtrsim 1$, this statement is valid, although the boundaries between attraction and repulsion get pushed to regions of γ and $\hat{\kappa}$ that are either impractical (too large density difference leads to rapid precipitation or creaming of even very small particles) or violate conditions such as $\gamma \ll 1$.

Further analysis shows that the almost horizontal phase boundaries in Fig. 3 for small γ are dominated by a sign change of F_ρ, which, to leading approximation for $|\hat{\kappa}| \ll 1$, is given by the condition $\lambda = 1$, translating into $\gamma = (3/32)^{1/2}\delta$. The horizontal dot-dashed lines in Fig. 3(c) demonstrate the accuracy of this approximation. The other boundary in the phase diagram results

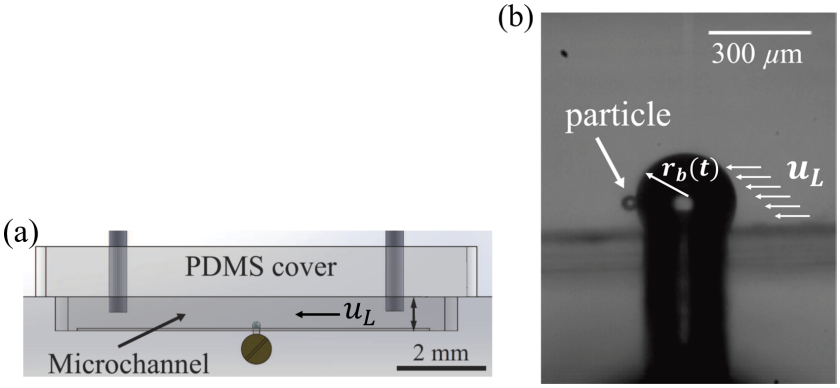

FIG. 4. Experimental setup (figure modified from Ref. [8]); (a) a spherical bubble is exposed to the microchannel flow u_L and driven to volumetric oscillations by a piezoelectric transducer; (b) a spherical particle is captured at a close distance to the bubble interface.

from balancing the leading order terms of F_ρ and $F_{i,2}$ for $\lambda \gg 1$ and $h_s \ll 1$, so that the radial coordinate is $r_s \approx 1 + 4\gamma$. This obtains a boundary governed by $\hat{\kappa}/(\hat{\kappa}+1) = 32\gamma^2/(1+4\gamma)^2$ independent of δ, which the dashed line in Fig. 3(c) proves to be an accurate prediction, almost indistinguishable from the numerically determined boundary for small δ.

IV. PARTICLES NEAR AN INTERFACE: COMPARISON WITH EXPERIMENT

In a recent study [8], a series of experiments were performed that approximate closely the simple scenario quantified in the previous section: A near-spherical microbubble ($a_b = 150\,\mu$m) was placed at the wall of a microfluidic chamber, and spherical polystyrene beads ($a_p = 30\,\mu$m, $\rho_p = 1050\,\mathrm{kg/m^3}$) were transported near the bubble by an imposed channel flow (water, $\rho_f = 1000\,\mathrm{kg/m^3}$); see Fig. 4(a). When the bubble was driven by a piezoelectric transducer ($f = 20$–36 kHz), it responded by nearly exclusively volumetric, small-amplitude oscillations (typically $\epsilon < 0.01$); this purely radial dynamics was intentionally set up to suppress streaming effects. Beyond a threshold ($\epsilon > \epsilon_c$), particles sufficiently close to the bubble were caught and transported to a stationary position very close to the bubble interface [Fig. 4(b)], from which they could be released by lowering ϵ below ϵ_c [37].

A. Polystyrene particle trapping and release

The channel flow past the bubble induces a steady flow component u_L around the bubble, exerting a drag on the particle, which by itself would transport the particle away from the bubble. It is the net attractive force from the rectified oscillatory flow that successfully counteracts the drag. Assessing the parameters for a typical experimental situation ($f = 29$ kHz results in $\lambda \approx 55$, while $\hat{\kappa} \approx 0.033$ and $\gamma \approx 0.05$, and thus $\delta \approx 0.022$), we find that, as expected, these parameter values lie well within the attractive regime predicted by the phase diagram from Eq. (6) for $u_L = 0$ as shown by the black dot in Fig. 3(a). To model this experimental scenario, we need to incorporate u_L, the flow field due to the channel flow, in Eq. (6). A strong enough u_L, or small enough ϵ, will move the boundary of the corresponding phase diagram such that the particle experiences repulsion instead of attraction.

B. Theory results

We model the flow field u_L as a low-Re steady flow around the bubble in the downstream (x) direction, obeying no-slip boundary conditions at the channel wall and no-stress at the bubble surface. The particle will be located at a height y_p above the wall, and the flow must asymptote

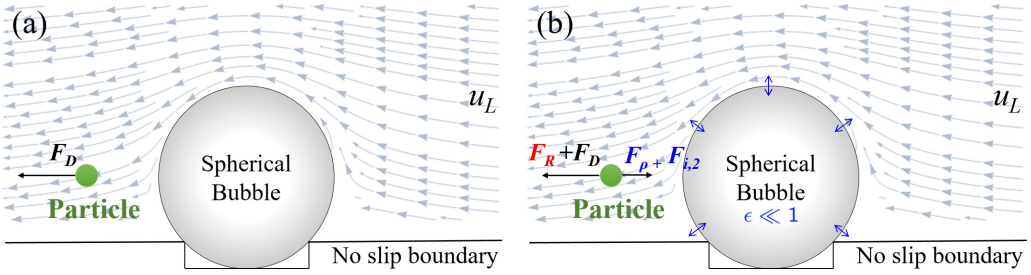

FIG. 5. (a) Computed flow field u_L around the quiescent bubble, indicating the drag F_D on the particle; (b) with volumetric bubble oscillations, the force balance from (6) determines particle position.

to the channel Poiseuille flow speed u_c in the downstream direction, $u_L(x \to \infty, y = y_p) = u_c$. From the rectangular channel dimensions, and the flow rate given in Ref. [8], a Poiseuille solution is constructed (see Refs. [38,39]) and the dimensional U_c at height $y_p a_b$ is obtained. Since the steady part of the flow field is defined as $\epsilon \tilde{u}_L(r)$ (see Sec. II B), this translates to $u_c = U_c/(\epsilon^2 a_b \omega)$; for the experiments on the release of particles we model here, the particle is situated $\approx 75\ \mu$m away from the wall, and the asymptotic speed is $U_c \approx 7.5$ mm/s.

Knowing u_c, the flow u_L is then constructed by taking into account the no-slip boundary condition at the wall exactly, while the no-stress condition at the bubble interface is satisfied approximately using singularity flow results from the literature [40–43]. Omitting some details, u_L is obtained analytically as a sum of Stokeslet, a stresslet, and their corresponding image systems along with a background linear shear flow that approximates the Poiseuille flow well near the wall (see Fig. 5). The height of the captured particle in experiment coincides closely with the location of the bubble equator (note the bubble is situated in a recessed pit), so that the drag force F_D acts under a small angle to the radial direction. The force is projected onto the r direction accordingly to balance it with those force components induced by the oscillatory flow.

All force terms in the slow-time equation (6) are now evaluated and plotted in Fig. 6(a) for the aforementioned experimental parameter values as a function of distance. The sum $F_\lambda + u_L$ is shown in Fig. 6(c), and zeros of this function mark equilibrium points with zero particle velocity. The repulsive force F_R leads, as expected, to the formation of a stable equilibrium at h_s, and the presence of F_D induces an unstable equilibrium at $h_u > h_s$. The value of h_s is insensitive to parameter changes within the range of experiments and translates to a submicron gap between bubble and particle at equilibrium, consistent with video material from Ref. [8]. Contrast this situation with a force balance that only contains the drag F_D and the acoustic far-field secondary radiation force approximation [15–17]

$$F_{SR} = -\frac{\lambda}{r^5}\left(\frac{\hat{\kappa}}{\hat{\kappa}+1}\right) \tag{9}$$

[Figs. 6(b) and 6(d)], as suggested in previous approaches [7,8]: while the attractive force values are of similar magnitude, there is no stable equilibrium at any finite distance from the bubble. The particle would be driven to contact with the bubble, contradicting the experiments.

The existence of a net attractive force for the range of gap $h_s < h < h_u$ explains the experiments that capture particles approaching the bubble sufficiently closely. While the minimum approach distance for capture was not quantified, the video data indicate that this distance is on the order of a few 10 μm, consistent with Fig. 6(c). The particle was released from the trapping when the bubble oscillation amplitude fell below $\epsilon_c \approx 0.006$ in experiment. This is easily tested within the model: the force balance suggested by Ref. [8] is plotted in Fig. 7(a) for different values of ϵ. The stable and unstable fixed points approach as ϵ is decreased and merge [at the analog of the phase boundary in Fig. 3(a)] when $\epsilon = \epsilon_c \approx 0.007$, in good agreement with the observed value. Unlike in Fig. 7(b), which again depicts the balance of F_D and F_{SR} only, our model shows that the equilibrium point is

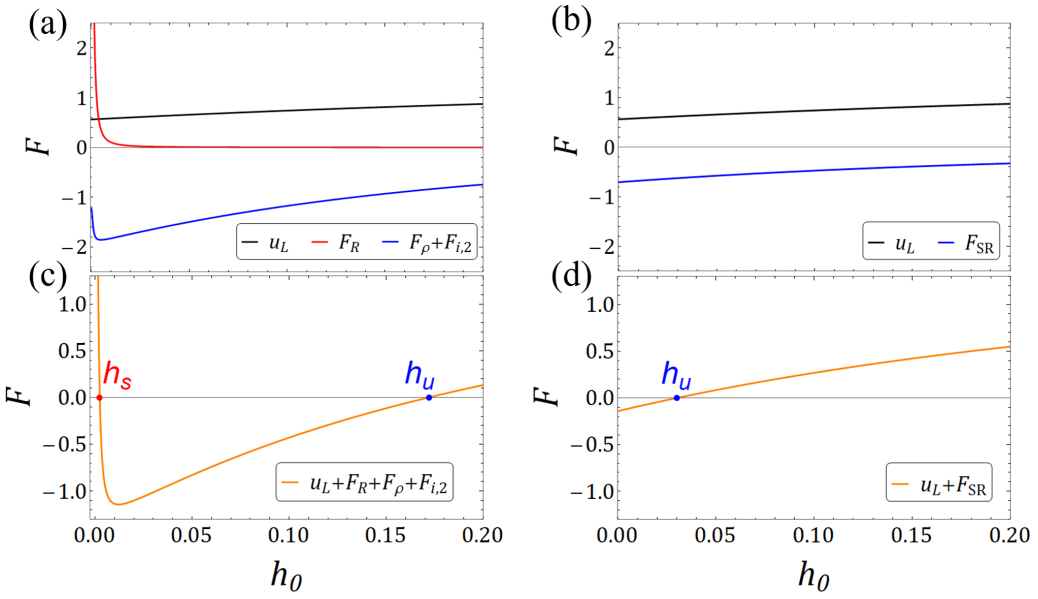

FIG. 6. Force contributions for $\lambda = 55$, $\gamma = 0.05$, $\hat{\kappa} = 0.033$ corresponding to the experiments with $\epsilon = 0.012$. The distance between bubble and particle surfaces h_0 is normalized by $a_b = 150\,\mu$m. (a) Forces from (6); (b) F_{SR} and u_L; (c) sum of forces in (a) showing two fixed points at h_s and h_u; (d) sum of forces in (b) resulting in only one unstable fixed point.

lost at a finite distance from the bubble surface as ϵ is decreased; dimensionally, the particle-bubble distance is still very small at this point, $h_0 \approx 1.5\,\mu$m. It should be noted that the magnitude of the modeled attractive force is significantly altered by the presence of the higher-order term $F_{i,2}$ for particles with these experimental parameters. Without it, the agreement with experiment would not be quantitative. The successful modeling for this particular $f = 29\,$kHz case translates directly to the other frequencies in the experimental range, as the dependence of ϵ_c on f in both experiment and theory is consistent with $\epsilon_c \propto 1/f$ [8]. This behavior can be deduced from the dominant balance of u_L and F_ρ, taking into account the scaling of u_L and λ with ϵ and $\omega = 2\pi f$.

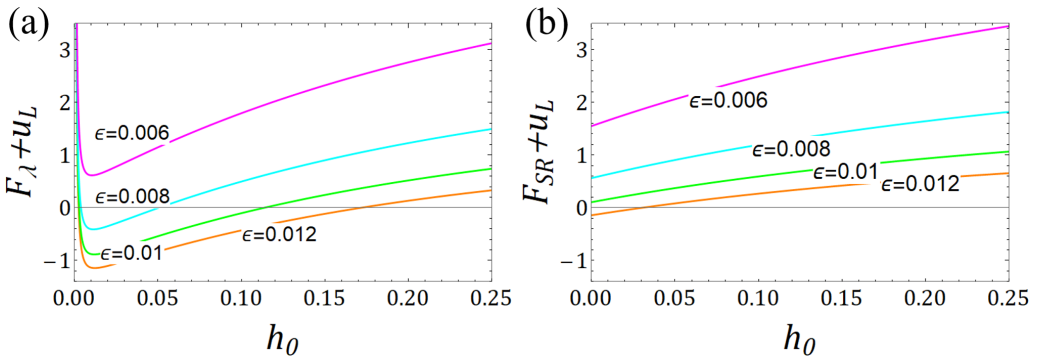

FIG. 7. Particle release. (a) Sum of forces from (6): as ϵ is decreased, the stable fixed point is lost at a finite distance from the bubble surface ($\epsilon_c \approx 0.007$ in agreement with experiment); (b) sum of F_{SR} and F_D: the unstable fixed point is lost at the bubble surface, and ϵ_c does not agree with the measured value.

V. PARTICLES AT LARGE DISTANCES: CONNECTION TO ACOUSTOFLUIDICS

The equations developed in Sec. II prove accurate both very close to the interface as well as at moderate distances and incorporate both viscous and inviscid effects. When the particle is at a large distance from the interface, the situation becomes analogous to SRF in acoustofluidics [4], where the particle is exposed to the oscillatory flow in a standing or traveling wave without a material boundary nearby. We note that there exist many well-established results in the inviscid limit of acoustofluidics, while in the opposite limit of strong viscous effects the recent literature gives contradictory results even for the direction of the force in certain situations [5,6,35].

The motivation for the present section is twofold: (1) we demonstrate that the Maxey-Riley-like approach outlined in this paper reduces to well-known results in acoustofluidics in the large distance limit and thus bridges the fields of acoustofluidics and inertial microfluidics; (2) we will shed light on the debate on the direction of viscous acoustofluidic forces. For definiteness, we shall compare the force on a particle in a spherical monopolar flow field (the $r \to \infty$ limit of the previous section) with that on a particle in a standing wave field. These results are expected to be equivalent except for effects of compressibility contrast between particle and fluid in the acoustofluidic case [4], resulting in monopole scattering, which cannot occur in our analysis of a rigid particle in incompressible flow. Since the particle is far away from boundaries, it becomes appropriate to include the viscous corrections mentioned in Sec. II A, which can be derived from the Basset-Boussinesq history force for translational oscillation in bulk. These corrections depend on the the viscous boundary layer thickness δ or, equivalently, its ratio to particle size $\delta_p = \delta/(n_B\gamma) = \sqrt{\frac{2}{3\lambda}}$. Explicitly, the hydrodynamic force (3) on the particle, in this far-field limit, becomes

$$\mathbf{F}^H \approx -6\pi\nu\rho_f a_p\left[\left(\frac{d\mathbf{r}_p}{dt}-\mathbf{u}\right)\left(1+\frac{1}{\delta_p}\right)\right]-\left(\frac{1}{2}+\frac{9}{4}\delta_p\right)m_f\left(\frac{d\mathbf{v}_p}{dt}-\frac{D\mathbf{u}}{Dt}\right)+m_f\frac{D\mathbf{u}}{Dt}. \tag{10}$$

Appropriate to the $r \to \infty$ limit, we have omitted the lubrication term and the higher-order inviscid correction. Note that the δ_p correction terms are of subleading order for either $\delta_p \ll 1$ or $\delta_p \gg 1$. The corrections are understood to be applied to the oscillatory terms of the particle and fluid velocities (for which a δ_p is defined) but not to the slow-time parts. As before, we render (10) dimensionless and perform timescale separation; the projection on the radial direction is natural in this limit (the radial axis connects the oscillator and the particle). The resulting slow-time equation is

$$\frac{dr_{p0}}{dT} = \hat{\kappa}\frac{u_0(r_{p0})u_0'(r_{p0})}{3\delta_p^2}\left\{\frac{(1+3\delta_p/2)(\hat{\kappa}+1+3\delta_p/2)-\left[3\delta_p^2/2(1+1/\delta_p)\right]^2}{(\hat{\kappa}+1+3\delta_p/2)^2+\left[3\delta_p^2/2(1+1/\delta_p)\right]^2}\right\}. \tag{11}$$

Here we have made use of the relation $\lambda = 2/(3\delta_p^2)$ to obtain a particle speed explicitly dependent on $\hat{\kappa}$ and δ_p. Interpreting the right-hand side as an effective far-field force F_f and normalizing by the secondary radiation force F_{SR} from (9), we obtain

$$\frac{F_f}{F_{SR}} = (\hat{\kappa}+1)\left\{\frac{(1+3\delta_p/2)(\hat{\kappa}+1+3\delta_p/2)-\left[3\delta_p^2/2(1+1/\delta_p)\right]^2}{(\hat{\kappa}+1+3\delta_p/2)^2+\left[3\delta_p^2/2(1+1/\delta_p)\right]^2}\right\}. \tag{12}$$

This ratio is depicted in Fig. 8; it asymptotes to 1 for $\delta_p \to 0$ independent of $\hat{\kappa}$, as expected, and shows a dramatic reversal of sign around $\delta_p \sim 1$. The asymptote at large δ_p depends on $\hat{\kappa}$ but approaches -1 for $|\hat{\kappa}| \ll 1$.

Also shown in Fig. 8 are two results from the acoustofluidics literature that both computed the contributions of monopole and dipole scattering from a spherical particle in a standing-wave field under the large sound wavelength assumption ($\lambda_w \gg a_p$) for arbitrary δ_p. Only the dipole part of those solutions is plotted, as effects of compressibility contrast are not present in the current situation. While Ref. [6] predicts a sign reversal like our approach, more recently Ref. [5], using a simplified formalism, argued that this result is unphysical. The qualitative agreement of our

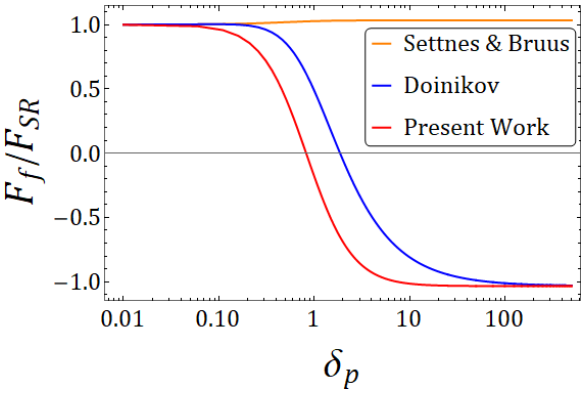

FIG. 8. Normalized force on a particle for large distances from the oscillation source, graphed as a function of $\delta_p = \sqrt{2\nu/(a_p^2\omega)}$ for $\hat{\kappa} = 0.033$ (corresponding to a polystytrene particle in water). The present work [Eq. (12)] predicts a sign change of the force as viscous effects become important, in agreement with Ref. [6] and contradicting Ref. [5].

independent Maxey-Riley like approach with Ref. [6] is obvious and can be further quantified: in the two limits, we obtain from (12)

$$F_{\delta_p\to 0} = F_{SR}\left[1 + \frac{3}{2}\left(\frac{\hat{\kappa}}{\hat{\kappa}+1}\right)\delta_p + O(\delta_p)^2\right], \tag{13a}$$

$$F_{\delta_p\to\infty} = -F_{SR}\left[(\hat{\kappa}+1) + O\left(\frac{1}{\delta_p}\right)^2\right]. \tag{13b}$$

The explicitly shown orders are in exact agreement with Ref. [6]. The approximations in our formalism do not simultaneously and systematically expand the viscous and inviscid force contributions and fail to pick up the $O(\delta_p^{-1})$ in the viscous limit. The theory of Ref. [5] omits several viscous effects, primarily because of the assumption of a potential flow in the far-field of the particle. While appropriate for the oscillatory flow, this assumption is inconsistent with the secondary (steady) flow, whose inertia is negligible and as a result does not have an inviscid far -field, i.e., viscous stresses are comparable with the fluid pressure [6,35]. In addition, Ref. [5] implicitly assumes that (1) the disturbance flow due to particle translation is weak, by neglecting self-interaction terms and (2) the disturbance flow due to the straining of the background flow is negligible. All of these assumptions are associated with viscous effects that are systematically accounted for in Refs. [6] and [35] and that are approximated by our current theory.

VI. CONCLUSIONS

A generalized model for inertial forces on particles in incompressible oscillatory flows was derived that takes into account the effect of an interface at any distance and can be applied for arbitrary viscous effects (δ_p values). Timescale separation of the oscillatory Maxey-Riley-like equation allows for a fast, simple calculation of forces leading to a formalism that provides simple predictions for the rectified migration of particles relative to a background flow field that is previously computed or measured and is an explicit input to the computation. Note that this steady particle displacement is different from any steady streaming displacement of the fluid elements; while there was no streaming in the particular (monopolar) flow fields quantified here, its presence does not affect the conclusions.

The parameter dependence of forces shows that even the simplest oscillatory flow fields can have both attractive and repulsive effects on particles depending on their relative density, their size relative to the interface scale and relative to the boundary layer thickness, as well as on the separation distance from the interface. Attraction eventually positions the particle at a stable equilibrium point that in many cases is much closer to the interface than any of the imposed scales of the problem. This makes the approach well suited for accumulating, concentrating, and accurate positioning of objects in microfluidic flow setups, including biological cells. For the latter, the finite stand-off distance from the interface furthermore prevents harmful exposure of the cells to a body of gas.

The regions of attraction and repulsion in the phase diagrams are governed primarily by the density-dependent inertial force F_ρ, which is a generalization of F_{SR} in acoustofluidics, showing a richer dependence on parameters and particle position. The δ dependence of the phase diagram also shows that a judicious choice of parameters allows for a transition from attractive to repulsive behavior or vice versa not only by changing the drag from an externally imposed flow or the amplitude of oscillation but also by changing the frequency of driving, which is usually the easiest to effect. Release of particles from capture thus becomes predictable and selectively tunable. We also demonstrate that near the interface there are always significant force contributions independent of density contrast, unlike what would be inferred from F_{SR} alone.

While the formalism opens up new possibilities for manipulation of microparticles very close to interfaces, it is also applicable to particles at a larger distance from the oscillating object. Then our approach agrees in both the viscous and inviscid limits with forces in acoustofluidic standing-wave fields, bridging inertial-force research in the acoustofluidic and microfluidic fields.

It should also be noted that the forces exerted on particles in the flow from oscillating interfaces can be considerably stronger—whether attractive or repulsive—than those in other inertial microfluidics (either shear-induced migration or acoustofluidics). Any (dimensional) inertial force in this context can be written as $\mathcal{F} \sim \rho U^2 a_p^2 f(\hat{\kappa}) g(a_p/L_u)$, where U^2 is a scale of squared flow velocity and g is a dimensionless function of particle size and characteristic flow length scale L_u. In inertial shear migration [1], U^2 is simply the square of the steady transport speed u_L, while in a channel of height H, $g = (a_p/H)^2$ or, near the wall of the channel, $g = (a_p/H)^4$; the $\hat{\kappa}$ dependence is weak in this case. For the radiation force $\mathcal{F}_{SR}$ of acoustofluidics, $U^2 = \langle u_w^2 \rangle$ with the oscillating fluid velocity in the wave u_w; furthermore, $g = a_p/\lambda_w$, using the wavelength λ_w, and (focusing on dipolar scattering) $f = \hat{\kappa}$. In the current work, we can write the dimensional rectification forces $\mathcal{F}_R$, $\mathcal{F}_\rho$, and $\mathcal{F}_{i,2}$ using $U^2 = \langle (\epsilon a_b \omega)^2 u_{\mathrm{osc}}^2 \rangle$ and $g = a_p/a_b$. $\mathcal{F}_\rho$, as an analog of $\mathcal{F}_{SR}$, shares the proportionality $f = \hat{\kappa}$, while the other contributions are approximately or exactly $\hat{\kappa}$-independent. Compared with shear migration, the forces described here scale more favorably with a_p and are larger because of the smaller scale $a_b < H$. The oscillatory velocity scale can easily exceed either typical transport speeds or fluid speeds in acoustic waves (also, $a_b < \lambda_w$ in many cases for practical parameters).

Furthermore, a different oscillation behavior of the interface [different $u_0(r)$] will give rise to different positional dependence of the forces, opening more versatile options for the capture and manipulation of particle position. The interface does not need to be a bubble; oscillating membranes or solid objects on the microscale (see Refs. [44,45]) are other possibilities. Exploiting these advantages should lead to exciting applications for a variety of tasks in microfluidics: from trapping and concentrating, to controlled release, to simultaneous size segregation and transport. The last task involves generalizing the current theory to higher-dimensional flows, which will be described in a later publication.

ACKNOWLEDGMENTS

The authors are indebted to Sungyon Lee for sharing experimental data and video information. Illuminating discussions with Stephen H. Davis and Howard A. Stone are gratefully acknowledged. S.A. acknowledges support from the National Science Foundation under Grants No. 1236141 and No. 1504301.

APPENDIX: MULTIPLE SCALE ANALYSIS FOR PURELY RADIAL OSCILLATIONS

We project (4) onto the radial direction to obtain a second-order nonlinear ODE for the particle position,

$$\lambda(\hat{\kappa}+1)\frac{d^2 r_p}{dt^2} + \left\{1 + H\left[\frac{X-\epsilon\Delta R(t)}{\delta}\right]\frac{\gamma}{X-\epsilon\Delta R(t)}\right\}\frac{dr_p}{dt}$$
$$= \epsilon\left\{\lambda\left(\frac{\partial u}{\partial t} + \epsilon u\frac{\partial u}{\partial r}\right) + \frac{2}{9}\epsilon\lambda n_B^2\gamma^2\left[\frac{2u}{r_p^2}\left(\frac{\partial u}{\partial r} - \frac{u}{r_p}\right) + \frac{\partial u}{\partial r}\frac{\partial^2 u}{\partial r^2}\right]\right.$$
$$\left. + u + H\left[\frac{X-\epsilon\Delta R(t)}{\delta}\right]\frac{\gamma\dot{\Delta R}}{X-\epsilon\Delta R(t)}\right\}_{r_p}, \tag{A1}$$

subject to initial conditions:

$$r_p(0) = r_{p_i}, \tag{A2a}$$
$$\left.\frac{dr_p}{dt}\right|_{t=0} = \epsilon V_i, \tag{A2b}$$

where $r_b = 1 + \epsilon\Delta R(t)$, $u_b = \frac{1}{\epsilon}\frac{dr_b}{dt} = \dot{\Delta R}$, $X = r_p - 1 - n_B\gamma$ is the gap between particle and mean position of the interface, and $H(z) = \exp[-z]$ enforces a decay of the lubrication drag on the order of boundary layer thickness distance away from the interface. Additionally, we decompose $u = u_{\text{osc}}(r,t) + \epsilon u_L$, which is appropriate for radial oscillatory flows with a slow steady component. Assuming all parameters are $O(1)$ and $\epsilon \ll 1$, we introduce a "slow time" $T = \epsilon^2 t$, in addition to the "fast time" t. Using the transformations

$$r_p(t) \mapsto r_p(t,T), \tag{A3a}$$
$$\frac{d}{dt} \mapsto \frac{\partial}{\partial t} + \epsilon^2\frac{\partial}{\partial T}, \tag{A3b}$$
$$\frac{d^2}{dt^2} \mapsto \frac{\partial^2}{\partial t^2} + 2\epsilon^2\frac{\partial^2}{\partial t\partial T} + \epsilon^4\frac{\partial^2}{\partial T^2}, \tag{A3c}$$

we seek a perturbation solution in the general form $r_p(t,T) = r_{p_0}(t,T) + \epsilon r_{p_1}(t,T) + \epsilon^2 r_{p_2}(t,T) + \cdots$ and separate orders of ϵ. At $O(1)$, the equation is

$$\lambda(\hat{\kappa}+1)\frac{\partial^2 r_{p_0}}{\partial t^2} + \left[1 + H_0\frac{\gamma}{h_0}\right]\frac{\partial r_{p_0}}{\partial t} = 0 \tag{A4}$$

with initial conditions,

$$r_{p_0}(0,0) = r_{p_i}, \tag{A5a}$$
$$\left.\frac{\partial r_{p_0}}{\partial t}\right|_{(0,0)} = 0, \tag{A5b}$$

where we have written $h_0 \equiv X_0 = r_{p_0} - 1 - n_B\gamma$ and expanded $H(h/\delta) = H(h_0/\delta) + (\epsilon/\delta)(r_{p_1} - \Delta R)H'(h_0/\delta) + \cdots \equiv H_0 + (\epsilon/\delta)(r_{p_1} - \Delta R)H_0' + \cdots$. Equation (A4) just means that $O(1)$ changes in particle position only occur over the slow timescale T or, in other words, $r_{p_0}(t,T) = r_{p_0}(T)$ with $r_{p_0}(0) = r_{p_i}$.

Going to $O(\epsilon)$, one obtains

$$\lambda(\hat{\kappa}+1)\frac{\partial^2 r_{p_1}}{\partial t^2} + \left(1 + H_0\frac{\gamma}{h_0}\right)\frac{\partial r_{p_1}}{\partial t} = \left[\lambda\frac{\partial u_{\text{osc}}}{\partial t} + u_{\text{osc}} + H_0\frac{\gamma}{h_0}\dot{\Delta R}\right]_{r_{p_0}}. \tag{A6}$$

Letting $u_{\rm osc}(r,t) = u(r)e^{it}$, $\Delta R = -ie^{it}$, and $\dot{\Delta R} = e^{it}$, the ensuing linear ODE is solved explicitly by

$$r_{p_1}(t,T) = -i[u(r_{p_0}) + w(r_{p_0})]e^{it} + A_1(T)\left(1 - e^{-\frac{h_0+H_0\gamma}{\lambda(\hat{\kappa}+1)h_0}t}\right) + B_1(T), \tag{A7}$$

where

$$w = -\frac{\gamma H_0(u-1) + iu\hat{\kappa}\lambda h_0}{h_0 + \gamma H_0 + i(\hat{\kappa}+1)\lambda h_0}. \tag{A8}$$

The general solution $r_{p_1}(t,T)$ satisfies the initial conditions if

$$A_1(0) = \frac{\lambda(\hat{\kappa}+1)h_0}{h_0+\gamma H_0}[V_i - u(r_{p_0}) - w(r_{p_0})]_{T=0}, \tag{A9a}$$

$$B_1(0) = i[u(r_{p_0}) + w(r_{p_0})]_{T=0}. \tag{A9b}$$

For $|\hat{\kappa}| \ll 1$, transients decay on a scale of $t = O(\lambda)$, corresponding to $O(\lambda/(2\pi)) \lesssim 10$ oscillation cycles for the typical experimental parameters in Sec. IV. We note that this time corresponds to $T = O(\epsilon^2\lambda) \ll \epsilon\lambda \ll 1$ (small Stokes number), making transients negligible on the slow timescales of interest. The oscillatory part of r_{p_1} can be, more generally, written as

$$\bar{r}_{p_1} = -i[u(r_{p_0}) + w(r_{p_0})]e^{it} = \int [u_{\rm osc}(r_{p_0}) + w_{\rm osc}(r_{p_0})]\,dt. \tag{A10}$$

With both initial conditions satisfied and ignoring transients, the equation at $O(\epsilon^2)$ after some rearrangement reads

$$\begin{aligned}
&\lambda(\hat{\kappa}+1)\frac{\partial^2 r_{p_2}}{\partial t^2} + \left(1 + H_0\frac{\gamma}{h_0}\right)\frac{\partial r_{p_2}}{\partial t} + \left(1 + H_0\frac{\gamma}{h_0}\right)\frac{\partial r_{p_0}}{\partial T} \\
&= \left\{u_L + \bar{r}_{p_1}\frac{\partial}{\partial r}\left(\lambda\frac{\partial u_{\rm osc}}{\partial r} + u_{\rm osc}\right) + \frac{2}{9}\lambda n_B^2\gamma^2\left[\frac{2u_{\rm osc}}{r^2}\left(\frac{\partial u_{\rm osc}}{\partial r} - \frac{u_{\rm osc}}{r}\right) + \frac{\partial u_{\rm osc}}{\partial r}\frac{\partial^2 u_{\rm osc}}{\partial r^2}\right]\right. \\
&\quad \left. + \frac{\gamma}{h_0}\left(\frac{H_0}{h_0} - \frac{H_0'}{\delta}\right)\frac{\partial}{\partial t}\left[\frac{(\Delta R - \bar{r}_{p_1})^2}{2}\right] + \lambda\left(u_{\rm osc}\frac{\partial u_{\rm osc}}{\partial r}\right)\right\}_{r_{p_0}}.
\end{aligned} \tag{A11}$$

The slow-time (t independent) dynamics are obtained by performing a time average of (A11) over a fast-time oscillation cycle. As a consequence, only terms involving slow-time (T) and products of first-order fast-time (t) quantities survive, and the resulting time-averaged equation reduces to the following explicitly computable form:

$$\begin{aligned}
\left(1 + H_0\frac{\gamma}{h_0}\right)\frac{\partial r_{p_0}}{\partial T} &= u_L(r_{p_0}) + \left\langle\left[\int w_{\rm osc}(r_{p_0})\,dt\right]\frac{\partial}{\partial r}\left(\lambda\frac{\partial u_{\rm osc}}{\partial t} + u_{\rm osc}\right)\right\rangle_{r_{p_0}} \\
&\quad + \frac{2}{9}\lambda n_B^2\gamma^2\left\langle\frac{2u_{\rm osc}}{r^2}\left(\frac{\partial u_{\rm osc}}{\partial r} - \frac{u_{\rm osc}}{r}\right) + \frac{\partial u_{\rm osc}}{\partial r}\frac{\partial^2 u_{\rm osc}}{\partial r^2}\right\rangle_{r_{p_0}} \\
&\quad + \frac{\gamma}{h_0}\left(\frac{H_0}{h_0} - \frac{H_0'}{\delta}\right)\overbrace{\frac{\partial}{\partial t}\left\langle\frac{(\Delta R - \bar{r}_{p_1})^2}{2}\right\rangle}^{\text{identically 0}} + \lambda\overbrace{\frac{\partial}{\partial t}\left\langle\left[\int u_{\rm osc}(r_{p_0})\,dt\right]\frac{\partial u_{\rm osc}}{\partial r}\right\rangle}^{\text{identically 0}} \\
&\quad + \overbrace{\left\langle\left[\int u_{\rm osc}(r_{p_0})\,dt\right]\frac{\partial u_{\rm osc}}{\partial r}\right\rangle}^{\text{Fluid Stokes drift = 0 for monopole}}.
\end{aligned} \tag{A12}$$

The nonzero time averages on the RHS of the above equation can be conveniently computed using complex variables, and after making appropriate substitutions, Eq. (6) follows.

[1] D. Di Carlo, D. Irimia, R. G. Tompkins, and M. Toner, Continuous inertial focusing, ordering, and separation of particles in microchannels, Proc. Natl. Acad. Sci. USA **104**, 18892 (2007).
[2] M. E. Warkiani, A. K. P. Tay, B. L. Khoo, X. Xiaofeng, J. Han, and C. T. Lim, Malaria detection using inertial microfluidics, Lab Chip **15**, 1101 (2015).
[3] L. Schmid, D. A. Weitz, and T. Franke, Sorting drops and cells with acoustics: acoustic microfluidic fluorescence-activated cell sorter, Lab Chip **14**, 3710 (2014).
[4] H. Bruus, Acoustofluidics 7: The acoustic radiation force on small particles, Lab Chip **12**, 1014 (2012).
[5] M. Settnes and H. Bruus, Forces acting on a small particle in an acoustical field in a viscous fluid, Phys. Rev. E **85**, 016327 (2012).
[6] A. A. Doinikov, Acoustic radiation pressure on a rigid sphere in a viscous fluid, Proc. R. Soc. Lond. A **447**, 447 (1994).
[7] P. Rogers and A. Neild, Selective particle trapping using an oscillating microbubble, Lab Chip **11**, 3710 (2011).
[8] Y. Chen, Z. Fang, B. Merritt, D. Strack, J. Xu, and S. Lee, Onset of particle trapping and release via acoustic bubbles, Lab Chip **16**, 3024 (2016).
[9] Il Song Park, J. H. Shin, Y. R. Lee, and S. K. Chung, On-chip micromanipulation using a magnetically driven micromanipulator with an acoustically oscillating bubble, Sensors Actuators A **248**, 214 (2016).
[10] R. Thameem, B. Rallabandi, and S. Hilgenfeldt, Particle migration and sorting in microbubble streaming flows, Biomicrofluidics **10**, 014124 (2016).
[11] C. Wang, B. Rallabandi, and S. Hilgenfeldt, Frequency dependence and frequency control of microbubble streaming flows, Phys. Fluids **25**, 022002 (2013).
[12] C. Wang, S. V. Jalikop, and S. Hilgenfeldt, Efficient manipulation of microparticles in bubble streaming flows, Biomicrofluidics **6**, 012801 (2012).
[13] C. Wang, S. V. Jalikop, and S. Hilgenfeldt, Size-sensitive sorting of microparticles through control of flow geometry, Appl. Phys. Lett. **99**, 034101 (2011).
[14] D. Ahmed, M. Lu, A. Nourhani, P. E. Lammert, Z. Stratton, H. S. Muddana, V. H. Crespi, and T. J. Huang, Selectively manipulable acoustic-powered microswimmers, Sci. Rep. **5**, 9744 (2015).
[15] V. Bjerknes, *Fields of Force* (Columbia University Press, New York, 1906).
[16] T. A. Hay, M. F. Hamilton, Y. A. Ilinskii, and E. A. Zabolotskaya, Model of coupled pulsation and translation of a gas bubble and rigid particle, J. Acoust. Soc. Am. **125**, 1331 (2009).
[17] W. T. Coakley and W. L. Nyborg, Cavitation; dynamics of gas bubbles; applications, in *Ultrasound: Its Applications in Medicine and Biology*, Vol. 3 of Methods and Phenomena, Their applications in science and technology, edited by F. J. Fry (Elsevier, North Holland, 1978).
[18] A. Hashmi, G. Yu, M. Reilly-Collette, G. Heiman, and J. Xu, Oscillating bubbles: A versatile tool for laboratory on a chip applications, Lab Chip **12**, 4216 (2012).
[19] Y. Chen and S. Lee, Manipulation of biological objects using acoustic bubbles: A review, Integr. Comp. Biol. **54**, 959 (2014).
[20] A. A. Doinikov and S. T. Zavtrak, Interaction force between a bubble and a solid particle in a sound field, Ultrasonics **34**, 807 (1996).
[21] L. A. Ostrovsky and Y. A. Stepanyants, *Dynamics of Particles and Bubbles under the Action of Acoustic Radiation Force* (Springer, Cham, 2018), pp. 205–230.
[22] R. Thameem, B. Rallabandi, and S. Hilgenfeldt, Fast inertial particle manipulation in oscillating flows, Phys. Rev. Fluids **2**, 052001 (2017).
[23] M. R. Maxey and J. J. Riley, Equation of motion for a small rigid sphere in a nonuniform flow, Phys. Fluids **26**, 883 (1983).
[24] D. Lhuillier, On the equation of motion of a rigid sphere in a non uniform and accelerated inviscid fluid. incidence on two-phase flow equations, Mech. Res. Commun. **9**, 295 (1982).
[25] H. Brenner, The slow motion of a sphere through a viscous fluid towards a plane surface, Chem. Eng. Sci. **16**, 242 (1961).
[26] K. Chong, S. D. Kelly, S. T. Smith, and J. D. Eldredge, Transport of inertial particles by viscous streaming in arrays of oscillating probes, Phys. Rev. E **93**, 013109 (2016).

[27] J. Feng, P. Ganatos, and S. Weinbaum, Motion of a sphere near planar confining boundaries in a Brinkman medium, J. Fluid Mech. **375**, 265 (1998).
[28] R. J. Clarke, S. M. Cox, P. M. Williams, and O. E. Jensen, The drag on a microcantilever oscillating near a wall, J. Fluid Mech. **545**, 397 (2005).
[29] A. A. Doinikov and A. Bouakaz, Effect of a distant rigid wall on microstreaming generated by an acoustically driven gas bubble, J. Fluid Mech. **742**, 425 (2014).
[30] A. Maali, R. Boisgard, H. Chraibi, Z. Zhang, H. Kellay, and A. Würger, Viscoelastic Drag Forces and Crossover from No-Slip to Slip Boundary Conditions for Flow Near Air-Water Interfaces, Phys. Rev. Lett. **118**, 084501 (2017).
[31] K. Chong, S. D. Kelly, S. Smith, and J. D. Eldredge, Inertial particle trapping in viscous streaming, Phys. Fluids **25**, 033602 (2013).
[32] E. E. Michaelides, The transient equation of motion for particles, bubbles, and droplets, J. Fluids Eng. **119**, 233 (1997).
[33] M. R. Maxey, The motion of small spherical particles in a cellular flow field, Phys. Fluids **30**, 1915 (1987).
[34] L. D. Landau and E. M. Lifshitz, *Course of Theoretical Physics, vol. 6, Fluid Mechanics* (Pergamon Press, Oxford, 1959).
[35] S. D. Danilov and M. A. Mironov, Mean force on a small sphere in a sound field in a viscous fluid, J. Acoust. Soc. Am. **107**, 143 (2000).
[36] M. S. Longuet-Higgins, Viscous streaming from an oscillating spherical bubble, Proc. Roy. Soc. A **454**, 725 (1998).
[37] We are grateful to Prof. Lee and her group for making the data set from this experiment available to us.
[38] H. A. Stone, Introduction to fluid dynamics for microfluidic flows, in *CMOS Biotechnology*, edited by H. Lee, D. Ham, and R. M. Westervelt (Springer, Boston, 2007), pp. 5–30.
[39] N. A. Mortensen, F. Okkels, and H. Bruus, Reexamination of Hagen-Poiseuille flow: Shape dependence of the hydraulic resistance in microchannels, Phys. Rev. E **71**, 057301 (2005).
[40] J. R. Blake, A note on the image system for a stokeslet in a no-slip boundary, Math. Proc. Cambridge Philos. Soc. **70**, 303 (1971).
[41] J. R. Blake and A. T. Chwang, Fundamental singularities of viscous flow, J. Eng. Math. **8**, 23 (1974).
[42] W. H. Mitchell and S. E. Spagnolie, Sedimentation of spheroidal bodies near walls in viscous fluids: Glancing, reversing, tumbling and sliding, J. Fluid Mech. **772**, 600 (2015).
[43] S. Kim and S. J. Karrila, *Microhydrodynamics: Principles and Selected Applications* (Dover Publication, 2013).
[44] B. R. Lutz, J. Chen, and D. T. Schwartz, Microfluidics without microfabrication, Proc. Natl. Acad. Sci. USA **100**, 4395 (2003).
[45] T. Açıkalın, A. Raman, and S. V. Garimella, Two-dimensional streaming flows induced by resonating, thin beams, J. Acoust. Soc. Am. **114**, 1785 (2003).